Journal of Atmospheric and Solar–Terrestrial Physics 227 (2022) 105804

Contents lists available at ScienceDirect

Journal of Atmospheric and Solar-Terrestrial Physics

journal homepage: www.elsevier.com/locate/jastp

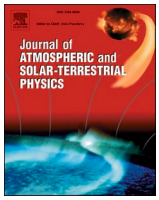

Research Paper

Elevated stratopause events in the current and a future climate: A chemistry-climate model study

Janice Scheffler [a,b], Blanca Ayarzagüena [a,c], Yvan J. Orsolini [d], Ulrike Langematz [a,*]

[a] Institut für Meteorologie, Freie Universität Berlin, Germany
[b] UK Centre for Ecology and Hydrology, Bush Estate, Penicuik, UK
[c] Departamento Física de la Tierra y Astrofísica, Universidad Complutense de Madrid, Spain
[d] NILU - Norwegian Institute for Air Research, Kjeller, Norway

ARTICLE INFO

Keywords:
Elevated stratopause events
Chemistry-climate model study
Future climate

ABSTRACT

The characteristics and driving mechanisms of Elevated Stratopause Events (ESEs) are examined in simulations of the ECHAM/MESSy Atmospheric Chemistry (EMAC) chemistry-climate model under present and projected climate conditions. ESEs develop after sudden stratospheric warmings (SSWs) in boreal winter. While the stratopause descends during SSWs, it is reformed at higher altitudes after the SSWs, leading to ESEs in years with a particularly high new stratopause. EMAC reproduces well the frequency and main characteristics of observed ESEs. ESEs occur in 24% of the winters, mostly after major SSWs. They develop in stable polar vortices due to a persistent tropospheric wave forcing leading to a prolonged zonal wind reversal in the lower stratosphere. By wave filtering, this enables a faster re-establishment of the mesospheric westerly jet, polar downwelling and a higher stratopause. We find the presence of a westward-propagating wavenumber-1 planetary wave in the mesosphere following the onset, consistent with in-situ generation by large-scale instability. By the end of the 21st century, the number of ESEs is projected to increase, mainly due to a sinking of the original stratopause after strong tropospheric wave forcing and planetary wave dissipation at lower levels. Future ESEs develop preferably in more intense and cold polar vortices, and tend to be shorter. While in the current climate, planetary wavenumber-2 contributes to the forcing of ESEs, future wave forcing is dominated by wavenumber-1 activity as a result of climate change. Hence, a persistent wave forcing seems to be more relevant for the development of an ESE than the wavenumber decomposition of the forcing.

1. Introduction

The troposphere, the stratosphere and the mesosphere are dynamically coupled at high latitudes in winter. A prominent example of this coupling are Sudden Stratospheric Warmings (SSWs) when the wind and temperature structures of the polar stratosphere are disturbed (Labitzke, 1981; Baldwin et al., 2021). Often coinciding with SSWs are mesospheric coolings (e.g., Siskind et al., 2007; Ren et al., 2011) during which the mesospheric layers cool down due to changes in the driving of the mesospheric branch of the Brewer-Dobson circulation (BDC) by gravity waves. The BDC, which consists of the mean meridional residual circulation (RC) and quasi-horizontal mixing, controls the transport of air and trace constituents in the stratosphere and the mesosphere. In the stratosphere, the RC is characterized by rising motion in the tropics, poleward flow and descending motion at high latitudes. The mesospheric branch of the RC is characterized by rising motion at the summer pole, transport to the winter hemisphere and descending motion at the winter pole (e.g. Bönisch et al., 2011). Using a thermal criterion, the upper boundary of the stratosphere, the stratopause, is characterized by a maximum in temperature and is located at approximately 50 km. In contrast to the formation of the summer stratopause that is caused by warming due to the absorption of solar ultraviolet (UV) light by ozone molecules, the formation of the winter stratopause is caused by adiabatic warming due to the descent of air in the mesospheric branch of the RC (Hitchman et al., 1989). The transition from a radiatively controlled summer stratopause to a dynamically controlled winter stratopause occurs in late autumn. In the mesosphere, the RC is controlled by gravity waves (GWs), whose propagation is influenced by the mean flow and by planetary waves (PWs) (Plumb, 2002).

If the stratospheric polar vortex is disturbed, the conditions for the

* Corresponding author. Institut für Meteorologie, Freie Universität Berlin, Carl-Heinrich-Becker-Weg 6-10, D-12165, Berlin, Germany.
E-mail address: ulrike.langematz@met.fu-berlin.de (U. Langematz).

https://doi.org/10.1016/j.jastp.2021.105804
Received 25 May 2021; Received in revised form 23 September 2021; Accepted 10 November 2021
Available online 22 November 2021

propagation of PWs and GWs are modified. During an SSW, for example, the establishment of easterlies in the polar stratosphere prevents a further upward propagation of PWs into the stratosphere and alters the conditions for the propagation of non-orographic GWs into the mesosphere. This changes the driving of the RC by wave dissipation and thus its strength and direction. Due to these variations in the RC, a large vertical upward displacement of the stratopause can take place after some SSWs (e.g., Chandran et al., 2011). In general, the stratopause descends and warms with the descending air in the downward branch of the RC during an SSW (e.g., Braesicke and Langematz, 2000), while at the same time a mesospheric cooling takes place in the upward RC branch at higher altitudes. Around the time when the polar vortex is re-established in the upper stratosphere, a new stratopause forms at lower mesospheric heights. The newly-built stratopause then slowly descends to its climatological winter height. This phenomenon is denoted as Elevated Stratopause Event (ESE) and was first described for the winter 1971/72 by analyzing rocket soundings (Labitzke, 1972).

More detailed analyses of ESEs have become possible in recent years with the improvement of the spatial and temporal resolution of middle atmospheric satellite data. The evolution of ESEs has been examined in observational (e.g., Manney et al., 2008, 2009a, 2009b; Orsolini et al., 2010; France et al., 2012) and modeling studies with the Whole Atmosphere Community Climate Model (WACCM), either in free or specified-dynamics mode (e.g., Limpasuvan et al., 2012, 2016; Chandran et al., 2011, 2013a, b; France and Harvey, 2013; Orsolini et al., 2017), the KANTO high-resolution general circulation model (Tomikawa et al., 2012), or the Canadian Middle Atmosphere Model (CMAM) (e.g. McLandress et al., 2013). Chandran et al. (2013a) and Limpasuvan et al. (2016) found that ESEs mostly occur after major SSWs that have a prolonged wind reversal in the lower stratosphere. The roles of GWs and PWs in driving the RC and thus the stratopause height have been recently highlighted. Based on studies with WACCM, Limpasuvan et al. (2012, 2016) concluded that while the mesospheric RC is mostly driven by GWs before and after an ESE, PWs play an important role at its onset. However, Chandran et al. (2013a) found with the same model that while an enhancement of westward PW forcing is typically observed at the onset of ESEs, it is not present in all cases. Other studies found a strong amplitude of PW wavenumber 1 (PW1) at mesospheric levels around the onset of ESEs (e.g., Liu and Roble, 2002; Tomikawa et al., 2012). This PW1 propagates upward and encounters a critical layer in the mesosphere, where it breaks and contributes to the driving of a poleward downward RC in the wintertime polar mesosphere. Several theories have been proposed to explain the origin of this mesospheric PW1. Apart from the upward propagation from the troposphere which is rejected by recent studies (e.g., Tomikawa, 2010), other theories encompass in-situ generation due to GW filtering by zonally asymmetric disturbances (e.g., Smith, 2003), and in-situ generation through barotropic or baroclinic instability (e.g., Tomikawa, 2010; Tomikawa et al., 2012; Limpasuvan et al., 2012, 2016; Chandran et al., 2013a).

During ESEs the coupling between the mesosphere and stratosphere is altered mainly due to the changes in the downward branch of the RC. When the maximum in the downward branch of the RC is located at a higher altitude during the reformation of the stratopause during ESEs, there is a stronger transport of mesospheric air, characterized by low concentrations in water vapor (H_2O) and high concentrations in nitrous oxides ($NO_x = NO + NO_2$) and carbon monoxide (CO), into the re-established stratospheric polar vortex (e.g., Siskind et al., 2007; Orsolini et al., 2017; Manney et al., 2009b). The magnitude of the secondary ozone layer (90–95 km) decreases after a brief enhancement during the period of mesospheric cooling, and the tertiary ozone maximum (70–75 km) drops in height (Smith et al., 2009; Kvissel et al., 2012; Tweedy et al., 2013).

Given the relevance of the stratosphere for the climate system, future changes in its mean state and in the characteristics of major SSWs have been investigated during the last decade. In particular, a wide range of model studies have examined future changes in SSW mean frequency of occurrence (e.g., Charlton-Perez et al., 2008; McLandress and Shepherd, 2009; Mitchell et al., 2012; Karpechko and Manzini, 2012; Ayarzagüena et al., 2018, 2020) and timing (Ayarzagüena et al., 2013). However, a consensus could not be found. For instance, Mitchell et al. (2012) showed that while some chemistry-climate models (CCMs) project an increase in SSW frequency, others project a decrease and the model ensemble mean shows a small insignificant increase in SSWs. An analysis of 12 CCMs participating in the Chemistry-Climate Model Initiative (CCMI) did not find a statistically significant change in the frequency of SSWs over the 21st century, irrespective of the metric used for the identification of the event (Ayarzagüena et al., 2018). However, an individual model study with the ECHAM/MESSy Atmospheric Chemistry (EMAC) CCM suggested that – even without a significant future change in the mean frequency of SSWs – a significant shift of SSWs to mid and late winter might occur in the future, consistent with a different intra-seasonal polar stratospheric response to future climate change and declining ozone depleting substances (ODSs) (Ayarzagüena et al., 2013). Based on these projected stratospheric changes and given the connection between most ESEs and strong major SSWs, an analysis of possible changes in the characteristics of ESEs in a changing climate seems appropriate. For the first time, future changes in ESEs are investigated in this work.

The goal of this work is to investigate in detail the occurrence, main characteristics and driving mechanisms of ESEs in the EMAC CCM. Previous model studies so far were based on CCMs like WACCM (e.g., Limpasuvan et al., 2012; Chandran et al., 2013a) or CMAM (e.g. McLandress et al., 2013), or on the KANTO general circulation model (e.g., Tomikawa et al., 2012). These models and EMAC differ in terms of horizontal and vertical resolution, vertical domain, and included feedback processes. For instance, while WACCM is a CCM as EMAC, its vertical domain and number of vertical layers are higher than in EMAC. This will in particular affect the representation of PWs and GWs in the models, which are the main drivers of ESEs. A comparison between the models thus will help us to clarify the roles of the different wave types on the evolution of ESEs and to isolate the main characteristics of ESEs from model biases. The second focus of our study is to investigate future changes of ESEs in a climate that is expected by the end of the 21st century, with increased concentrations of greenhouse gases (GHGs) and a recovered stratospheric ozone layer.

The paper is organized as follows: Section 2 describes the EMAC CCM and the methods we applied in this study. The characteristics of ESEs in EMAC are described for the current climate in Section 3. Possible changes in ESE characteristics in a future climate are investigated in Section 4. A summary and a discussion are given in Section 5.

2. Model, data and methods

All simulations used in this study were run with the CCM EMAC. EMAC is a numerical chemistry and climate simulation system that includes submodels describing tropospheric and middle atmosphere processes (Jöckel et al., 2006). The core atmospheric model is the fifth-generation European Centre Hamburg general circulation model ECHAM5 (Roeckner et al., 2006). In this study, EMAC was run in the version ECHAM5.3.01/MESSy 1.7 at T42L39MA, i.e., with a spherical truncation of T42 (corresponding to a quadratic Gaussian grid of approximately 2.8° by 2.8° in latitude and longitude) and 39 levels in the vertical with a model top at 0.01 hPa (~80 km). The applied model setup composes the standard submodels for hydrological and radiative processes as well as homogeneous and heterogeneous chemical reactions (Sander et al., 2005), a short-wave radiation scheme with enhanced spectral resolution (Nissen et al., 2007), and orographic (Lott and Miller, 1997) and non-orographic (Hines, 1997a, b) gravity wave drag parameterizations. Only the non-orographic gravity wave drag (NGWD) is available as an output variable and shown in this study.

As will be discussed in more detail later, the model top at 80 km is located in the altitude range where ESEs form. While in the real

atmosphere ESEs may develop at levels higher than the EMAC model top, we find that our model is capable to simulate ESEs occurring below 80 km as well as the underlying dynamics for the reformation of the stratopause. A similar conclusion was made by Tomikawa et al. (2012) who showed that a model with a top at 85 km can be sufficient to model the dynamics of elevated stratopause events. In addition, even in models extending into the lower thermosphere, the stratopause reforms -on average- at lower altitudes than 80 km: near 75 km in the composite of 13 ESEs in SD-WACCM (extending up to 140 km) (Limpasuvan et al., 2016), or in the composite of 9 ESEs in SD-WACCM-X (extending up to 400 km) (Zhang et al., 2021).

Two time slice simulations are analyzed in this work: REF2000 representing the year 2000 and REF2095 representing the year 2095, each with 40 years of simulation for analysis. More information on the model, the experimental setup and the performance of the model can be found in Ayarzagüena et al. (2013), Oberländer et al. (2013), Meul et al. (2014), and Langematz et al. (2014). The runs do not contain natural forcing by solar variability and volcanoes. The quasi-biennial oscillation is not internally generated by the model in this resolution. Hence, tropical stratospheric zonal winds are weakly easterly. For the REF2000 simulation, observed mixing ratios of well-mixed GHGs (CO_2, CH_4, N_2O) and ODSs are prescribed from IPCC (2001) and WMO (2007), respectively. In the case of the REF2095 run, GHG concentrations for the year 2095 are taken from the IPCC SRES A1b scenario (IPCC, 2001) and ODS concentrations follow the WMO A1 scenario (WMO, 2007). Sea surface temperatures (SSTs) and sea-ice concentrations (SICs) are prescribed with output from simulations of the atmosphere-ocean general circulation model ECHAM5 Max-Planck-Institute Ocean Model (ECHAM5/MPIOM) (Jungclaus et al., 2006) as 10-year monthly means of 1995–2004 for the REF2000 and 2090–2099 for the REF2095 simulation.

Here, only major sudden stratospheric warmings (SSWs hereafter) are considered. They are detected according to the World Meteorological Organization (WMO) criterion, i.e. the simultaneous reversal of zonal mean zonal wind at 60°N and the zonal mean temperature gradient between 60°N and the pole at 10 hPa from November to March (Labitzke, 1981). Westerly wind at 10 hPa must persist for at least 10 consecutive days before a new event can be identified (corresponding to the radiative relaxation time scale (Newman and Rosenfield, 1997)). Stratospheric final warmings are excluded by requiring 10 days of westerly winds before 30 April and after the occurrence of the warming. Based on this criterion, Ayarzagüena et al. (2013) found a mean frequency of 8.5 and 10.3 events/decade in REF2000 and REF2095, respectively. More details about seasonality of the SSWs in the mentioned simulations and its changes in the future can be found in Ayarzagüena et al. (2013). If there are more than one SSW per winter, only the SSW with the strongest wind reversal is considered, i.e. the SSW with the highest deceleration of mean wind between 15 and 5 days prior to the SSW onset and 0–5 days after the SSW onset. By choosing only the strongest event in a winter we avoid biasing the composite analysis by including the same event repeatedly but at different timing. Additionally, SSWs were classified into two types according to the synoptic structure of the polar vortex: shifted off the pole (vortex displacement SSW) or broken into two parts (vortex split SSW). To perform this classification, an algorithm based on the analysis of the area-weighted rotation around the occurrence of the SSW (similar to that developed by Charlton and Polvani (2007)) was applied (Ayarzagüena et al., 2019).

For the determination of the stratopause, a thermal criterion was applied. The conventional criterion for the stratopause height, namely the temperature maximum in an appropriate height range, can be misleading after SSWs. When the mesospheric branch of the RC is disturbed, no clear stratopause is established and the upper stratosphere/lower mesosphere (USLM) region can show an isothermal temperature profile in the polar cap mean (70°–90°N) over a large altitude range. To avoid the detection of an isothermal temperature region as a stratopause, two conditions should be fulfilled. The stratopause is determined as the height where (1) the lapse rate of the area-weighted polar cap mean (70°–90°N) temperature decreases to −2 K/km or lower and does not increase again above this threshold at the next higher level, similar to the WMO definition of the tropopause (World Meteorological Organization, 1957), and (2) – to avoid isothermal layers – the difference between the temperature at the stratopause and at the next lower pressure level exceeds one standard deviation. A relative threshold for the daily change in stratopause height was applied, i.e., the strongest 0.5% of changes in the winter stratopause height. The use of a variable relative threshold accounts for differences in climatology when comparing different data sets or periods and allows for a consistent comparison across data sets. Further, the specific 0.5% value was chosen so that the order of magnitude of the stratopause jump in the REF2000 run would resemble that described by other studies (e.g. Chandran et al., 2013a). If there is more than one ESE per winter, the ESE with the highest change in stratopause height is chosen to avoid an overlapping of events when analyzing their temporal sequence. Changes in stratopause height related to the change of season are not considered as ESEs. Events where the newly-built stratopause was below the winter mean stratopause height were eliminated.

The comparison of the evolution of ESEs and SSWs that are not followed by an ESE (hereafter "SSW-only events") under present and future conditions is accomplished by an analysis of composite maps of different fields around the occurrence of both types of events. In the case of all ESE composites, day 0 corresponds to the day when the criterion for the identification of ESEs is fulfilled. For SSW-only events, day 0 is chosen as 14 days after the wind reversal at 10 hPa in both the REF2000 and REF2095 simulations. This 14-day period corresponds to the averaged time between the wind reversal and the occurrence of ESEs, and applies to both simulations. The selection of day 0 for SSW-only events (rather than the usual selection based on the reversal of zonal mean zonal wind) was done to enable a direct comparison with ESEs. In the composite maps of anomalous fields, anomalies are computed as the daily deviation of the field from the climatology of each calendar day in the corresponding simulation. This procedure removes the effects of a possible change in the timing of SSWs under different climate conditions, as the seasonal cycle is not included. The statistical significance of differences between the characteristics of ESEs and SSW-only events and differences in ESE properties between present and future conditions was determined with two-tailed Student's t-tests when population variances are unknown and not identical.

3. Elevated stratopause events in the current climate

We first focus on the properties of ESEs in the REF2000 simulation to assess the ability of EMAC to reproduce the specific characteristics of ESEs that have been identified in observations and previous model studies.

Table 1 displays the number of winters in which the different phenomena (ESEs, SSWs and SSWs-only) take place in EMAC. In the REF2000 simulation, 31 out of 38 analyzed winters show at least one SSW, i.e. 82% of the winters. With a threshold value for the stratopause height change of 8.43 km, ESEs occur in 9 out of 38 winters (24%). All ESEs occur after SSWs except for one event that follows a minor warming. In 22 out of 38 winters (58%) SSW-only events were detected.

Table 1
Number of winters when the different stratospheric events (major stratospheric warmings (all SSWs), elevated stratopause events (ESEs) and major stratospheric warmings not followed by ESEs (SSW-only events)) take place in the reference and the future simulations, REF2000 and REF2095, respectively. The percentage of winters out of the total is indicated in brackets for all SSWs, ESEs and SSW-only events. See text for the definition of each type of event.

Model run (nr of winters)	All SSWs	ESEs	SSWs-only
REF2000 (38)	31 (82)	9 (24)	22 (58)
REF2095 (39)	33 (85)	14 (36)	19 (49)

Regarding the type of SSWs, the ratio of vortex split SSWs to vortex displacement SSWs is 0.29 in ESEs and 0.38 in SSW-only events. Hence, the ratio of split to displacement events is lower in ESEs than in SSW-only events. This result disagrees with Chandran et al. (2013a), who find a predominance of split SSWs prior to ESEs. One reason for this disagreement and the low ratio of split to displacement SSWs compared to reanalysis (0.83 for JRA-55 in the satellite period 1979–2010) might be a much weaker planetary wavenumber-2 (PW2) wave activity in EMAC (Ayarzagüena et al., 2018).

In Fig. 1 we show height-time sections of (a) zonal mean temperature T, (b) zonal mean zonal wind $\overline{u}$, (c) Eliassen-Palm flux divergence *divEP*, (d) meridional component of the RC $\overline{v}^*$, (e) vertical component of the RC $\overline{w}^*$, and (f) non-orographic gravity wave drag NGWD for a composite of all ESEs. The EP flux divergence is a metric for the drag exerted on the zonal mean flow by the dissipation of model resolved waves (in the stratosphere essentially planetary waves), with positive values indicating an acceleration and negative values (EP flux convergence) indicating a deceleration of the westerly zonal mean zonal wind. The components of the RC are defined via the transformed Eulerian mean equations (e.g., Andrews et al., 1987). Fig. 2 shows the same quantities for SSW-only events. Anomalies from the 38-year climatology for these variables are shown in Fig. 3 for ESEs and Fig. 4 for SSW-only events.

ESEs in EMAC show specific characteristics that differ from SSW-only events and that, in most cases, are in agreement with Limpasuvan et al. (2016) and Chandran et al. (2013a):

1. The polar night jet starts to strongly decelerate in the mesosphere and upper stratosphere at about the same time (lag −40 days) for both types of events (Figs. 1b and 2b). While for SSW-only events this deceleration seems to be initiated in the upper mesosphere as early as 60 days before the event and then propagates downward (Figs. 2b and 4b), a weaker polar night jet is found in early winter (lag −60 days) at slightly lower altitudes (upper stratosphere/lower mesosphere) in the case of ESEs (Figs. 1b and 3b). As a result, easterly winds set in significantly earlier in the upper stratosphere for ESEs than for SSW-only events (Figs. 1b and 2b). Nevertheless, SSW-only events show significantly stronger easterly winds than ESEs between lag −20 and −10 days, indicating that the magnitude of the easterlies is not the critical factor for the evolution of an ESE.
2. The downward propagation of temperature and zonal wind structures in the lower stratosphere (LS) proceeds significantly slower in the case of ESEs than for SSW-only events (Figs. 1a, b and 2a, b). For SSW-only events, significantly stronger but shorter momentum forcing by resolved waves and enhanced downwelling further down in the middle atmosphere are found than for ESEs (Figs. 1c, e and 2c, e).
3. The zonal mean zonal wind in the stratosphere is reversed significantly longer for ESEs than for other SSWs. In the stratosphere above 10 hPa, the ESE composite shows a reversal of the zonal mean wind for about 14 days, while for SSW-only events a wind reversal of about 7 days is found (Figs. 1b and 2b).
4. During and after SSWs, the mesosphere cools, consistent with an anomalous upward residual velocity. Both the anomalous upwelling and the adiabatic cooling proceed downward with time, reaching the climatological stratopause at about 1 hPa around day 0 (i.e. when the mesosphere begins to warm again). These changes are found to be

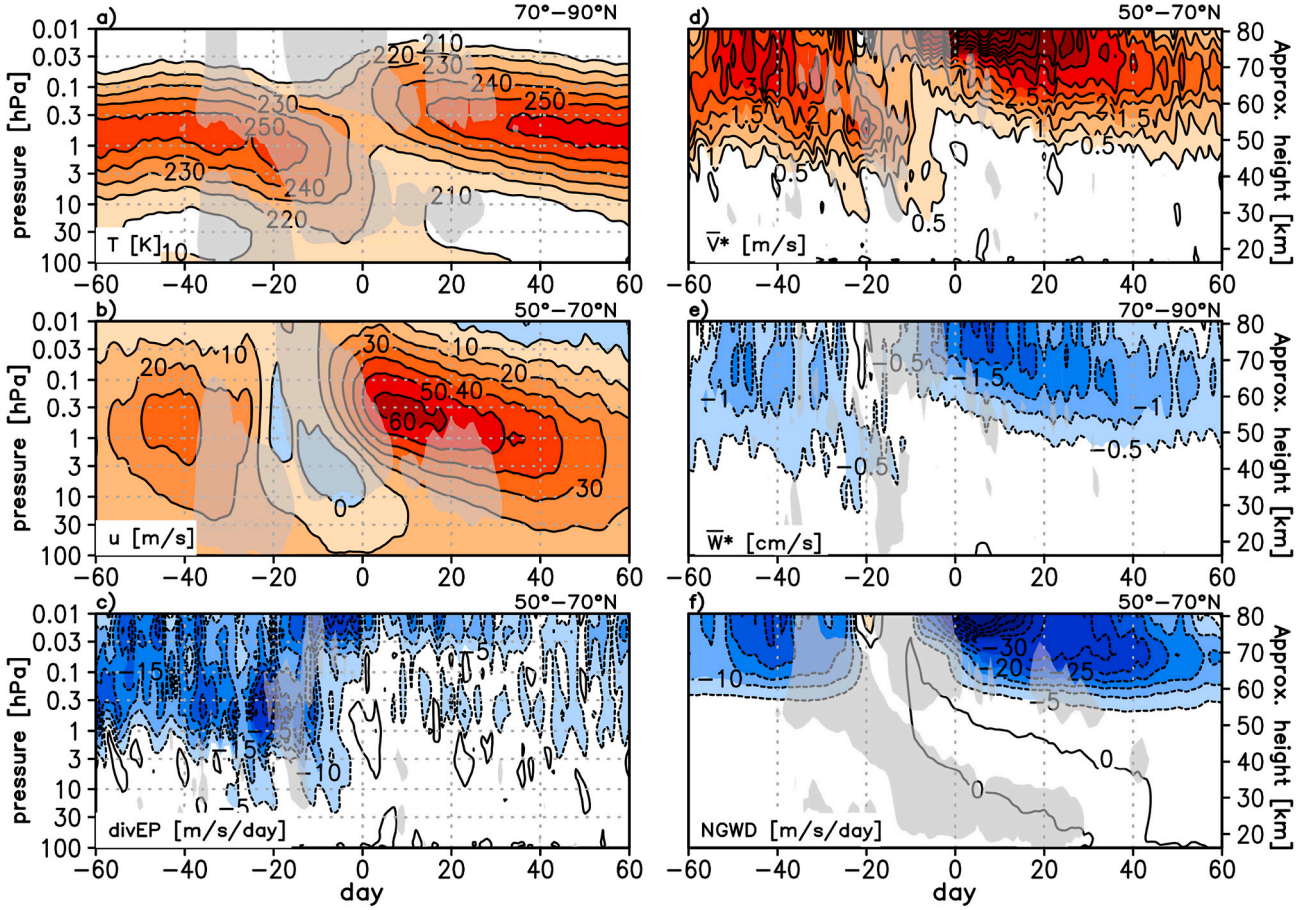

Fig. 1. ESE composites for the REF2000 simulation of a) zonal mean temperature [K], b) zonal mean zonal wind [m/s], c) EP flux divergence [m/s/day], d) $\overline{v}^*$ [m/s], e) $\overline{w}^*$ [cm/s], and f) non-orographic gravity wave drag NGWD [m/s/day]. Zonal mean temperature and $\overline{w}^*$ are shown at 70°–90°N, all other parameters at 50°–70°N. Gray shading denotes where the values for ESEs are statistically significantly different from SSW-only events at a 95% confidence level (Student's t-test).

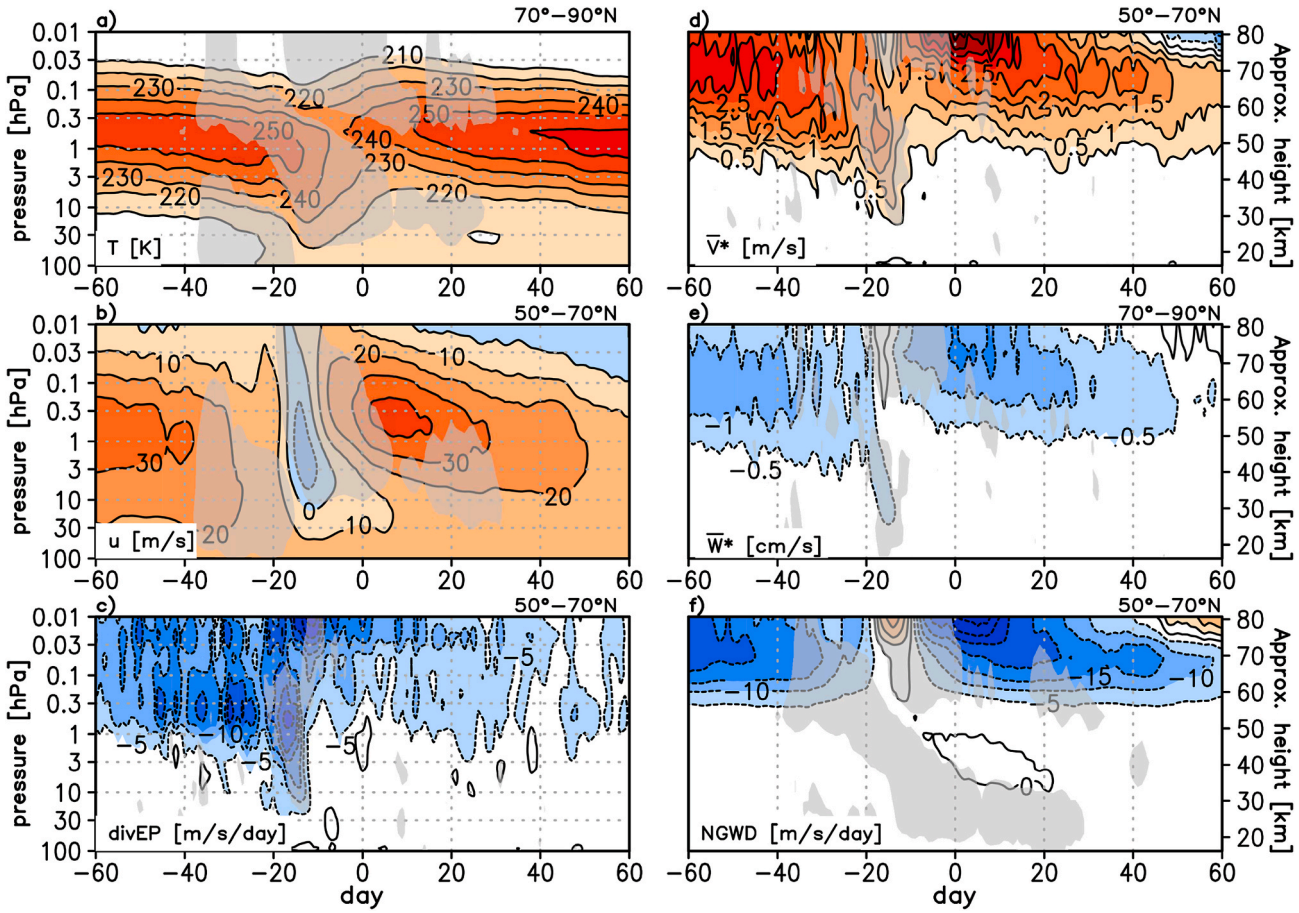

Fig. 2. As Fig. 1 but for SSW-only events.

significantly stronger in ESEs than in SSW-only events (Figs. 3a, e and 4a, e).

5. The reformed stratopause is located above the usual winter mean stratopause altitude for ESEs, ranging between 57 and 65 km height. (Fig. 1a). This is consistent with the larger and higher maximum in mesospheric downwelling after the events than before (Figs. 1e, 2e and 3e, 4e). In contrast, the reformation of the stratopause in SSW-only events takes place only slightly higher than its former altitude and close to the climatological winter stratopause height, on average at 53 km (Fig. 2a). A weak upward shift of the stratopause during SSW-only events was also documented by Chandran et al. (2013a).

3.1. Tropospheric forcing

Possible differences in the tropospheric forcing of ESEs in comparison with SSW-only events have been isolated by analyzing the time evolution of the anomalous meridional eddy heat flux at 100 hPa (HF100), averaged over the extra-tropics (45°–75°N). HF100 is a commonly used measure for the injection of tropospheric wave activity into the stratosphere (Hu and Tung, 2003). As seen in Fig. 5a, the anomalous HF100 is significantly stronger but shorter prior to day 0 for SSW-only events than ESEs, consistent with the differences found in the momentum forcing by resolved waves during SSWs (Figs. 3c and 4c). The shorter and more intense tropospheric forcing together with a preconditioned weak upper polar vortex explain the more abrupt and shorter appearance of strong easterlies from the mesosphere down to the stratosphere for SSW-only events, while the more persistent tropospheric wave forcing in the case of ESEs generates weaker easterlies first in the lower mesosphere and upper stratosphere, which then slowly propagate downward for 2–3 weeks. The longer-lasting tropospheric forcing before ESEs is due to a second pulse of wave activity with a contribution of PW2 that follows the first PW1-only pulse by about 15 days (Fig. 6a).

3.2. Residual circulation and wave drag

The analysis of the evolution of the RC and the exerted wave drag highlights other specific characteristics of ESEs. Having in mind that in the winter extra-tropical middle atmosphere the zonal momentum wave forcing is mainly balanced by the Coriolis term (Hitchman et al., 1989), we can relate an easterly wave drag at mid-latitudes to a poleward residual meridional velocity and downwelling at polar latitudes. In both ESEs and SSW-only events, we find a strengthening of the RC in the stratosphere (positive anomalies of $\bar{v}^*$ in Figs. 3d and 4d and negative anomalies of $\bar{w}^*$ in Figs. 3e and 4e) starting around lag −40. At about the same time, an equatorward and upward anomaly of the RC develops higher up in the mesosphere (Figs. 3d, e and 4d, e). These anomalies of opposite sign are induced by enhanced dissipation and westward drag by PWs (negative EP-flux divergence in Figs. 3c and 4c) in the stratosphere and by enhanced dissipation of NGWs and eastward drag (positive anomalies in Figs. 3f and 4f) in the mesosphere. The anomalous weakening of the climatological mesospheric RC is consistent with the mesospheric cooling and the re-establishment of the mesospheric westerly polar night jet (Figs. 3a, b and 4a, b). The described evolution of the RC and wave drag is common for both ESEs and SSW-only events. However, around day −15 SSW-only events show significantly shorter but stronger maxima of the RC acceleration and eastward NGWD than ESEs, which can be related to the more compact EP flux convergence and is consistent with the evolution of anomalous HF100 (Fig. 5a). The

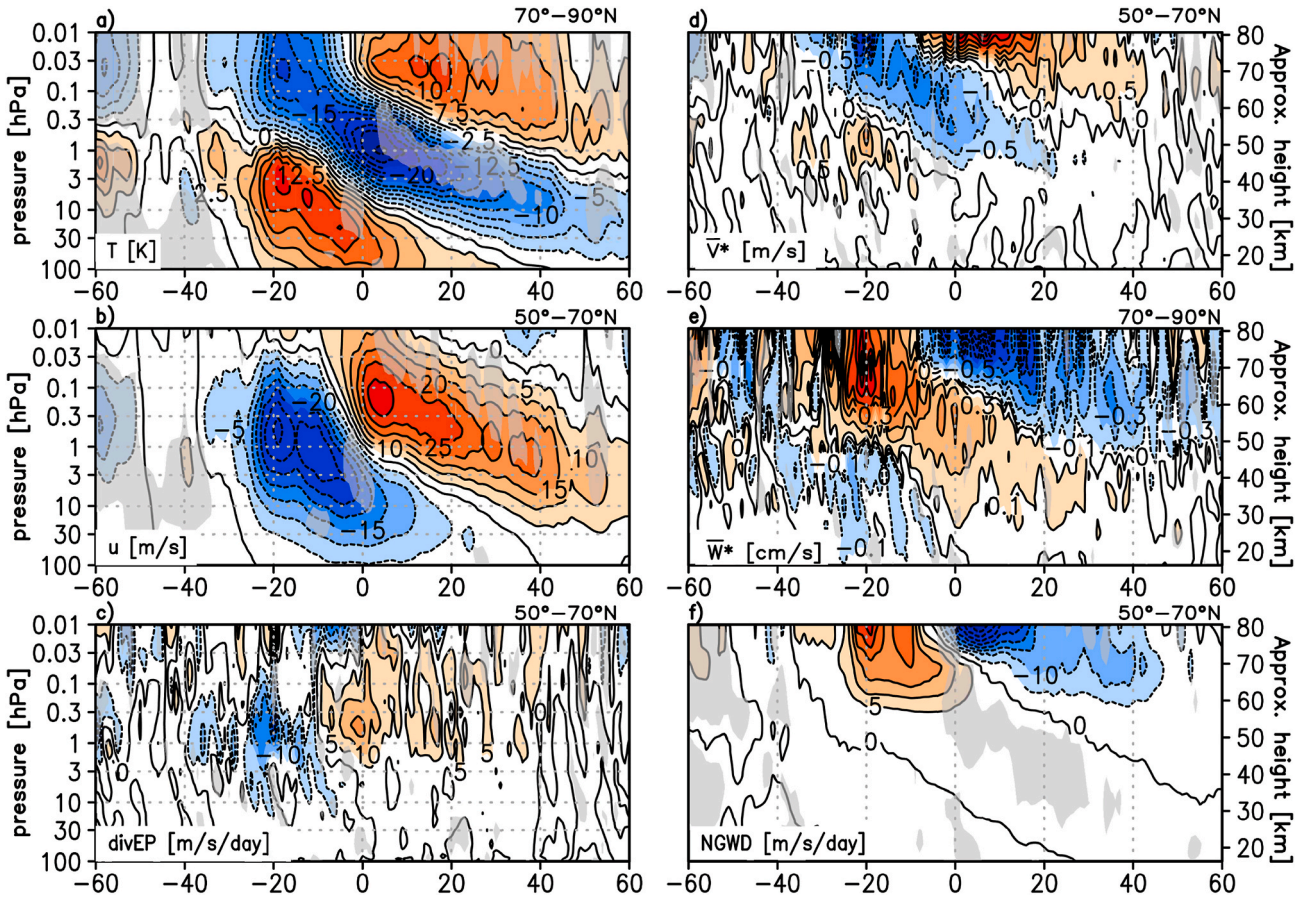

Fig. 3. As Fig. 1 but for the anomalies from the daily climatology of the fields. Gray shading shows where the anomalous ESE composite in the REF2000 simulation is significantly different (at a 95% confidence level) from the anomalous ESE composite in the REF2095 simulation (compare with Fig. 9) according to Student's t-test.

higher intensity of the EP flux convergence for SSW-only events induces significantly stronger easterlies that enable enhanced eastward NGWD; the shorter duration of the EP flux convergence favors an earlier re-establishment of the westerlies throughout the stratosphere and mesosphere in SSW-only events compared to ESEs.

Around 5 days prior to the ESE in the upper and middle mesosphere and 5 days after the ESE in the lower mesosphere, the anomalous RC changes its sign, as westward NGWD begins to dominate in the mesosphere, leading to the reformation of the climatological poleward and downward RC. The westward NGWD and thus the upper mesospheric RC are significantly stronger for ESEs than SSW-only events as a result of stronger mesospheric westerly winds (Figs. 1–4, d, e, f). Additionally, moderate negative anomalies of EP flux divergence are found in the upper mesosphere in the 10 days preceding ESEs (Figs. 3c and 4c), which slightly counteract the anomalous eastward NGWD and later support the evolution of anomalous westward NGWD and enhanced downwelling. This implies that, well prior to and after the ESE, the anomalous mesospheric RC is mainly driven by GWs, whereas around the ESE onset, PWs and GWs both contribute to the strengthening of the RC. This transition of the main providers for the westward drag from PWs around the ESE to NGWs thereafter is consistent with results from the GW-resolving GCM of Tomikawa et al. (2012). The WACCM-based studies also found both drivers for post-ESE downwelling but tend to show the PW drag peaking at higher altitudes (95–100 km) (Limpasuvan et al., 2012, 2016; Chandran et al., 2013a; Stray et al., 2015). One possible explanation for this altitude discrepancy is the location of the model top at 80 km in EMAC which allows only to simulate the lower part of this PW activity. Finally, around the onset of ESEs, strong positive anomalies of EP flux divergence around 1 hPa lead to a positive absolute EP flux divergence at that level resulting in a significantly faster and stronger re-establishment of the westerlies in the upper stratosphere than in the case of SSW-only events (Fig. 1b, c vs. 2b, c and Fig. 3b, c vs. 4b, c). The reasons for the anomalous EP flux divergence are presumably twofold. The easterlies occurring in the lower and middle stratosphere after the SSW prevent tropospheric PWs from upward propagation into the upper stratosphere and mesosphere. This is obvious in a decrease of the stratospheric amplitude of PW1 geopotential height between days −20 and 0 in both ESE and SSW-only events (Fig. 7a, b). Accordingly, the drag of PW1 on the zonal mean wind is reduced, as shown by the EP flux divergence in Fig. 1c. A second reason is in-situ instability, explored in the next section.

3.2.1. *Mesospheric PW1 generation*

A few days around the onset of ESEs and SSW-only events, a PW1 with strong amplitude forms in the mesosphere in the composites (Fig. 7a, b). However, for the ESE events, we see a double maximum at 20 hPa and 0.2 hPa with a decrease in amplitude in the mid and upper stratosphere implying that upward propagation of PW1 from the stratosphere can be excluded as a possible cause for the uppermost wave peak. Indeed, a westward-travelling PW1 in the lower mesosphere (0.2 hPa) is identified during the same time period, i.e. around −14 and −6 days before the onset of the ESEs (Fig. 8a). This travelling PW1 can be distinguished in Fig. 8a from the quasi-stationary waves that are present during the rest of the days. Thus, an amplification of PW1 in the USLM seems to occur prior to ESEs that has already been documented in the literature (e.g. Tomikawa et al., 2012; Limpasuvan et al., 2016) and is probably linked to barotropical and/or baroclinical shear instability (Hoskins et al., 1985). For the SSW-only composite, we do not find a double PW1 amplitude maximum in the LS and USLM but only one maximum in the USLM close to day 0 (Fig. 7b). This implies that the

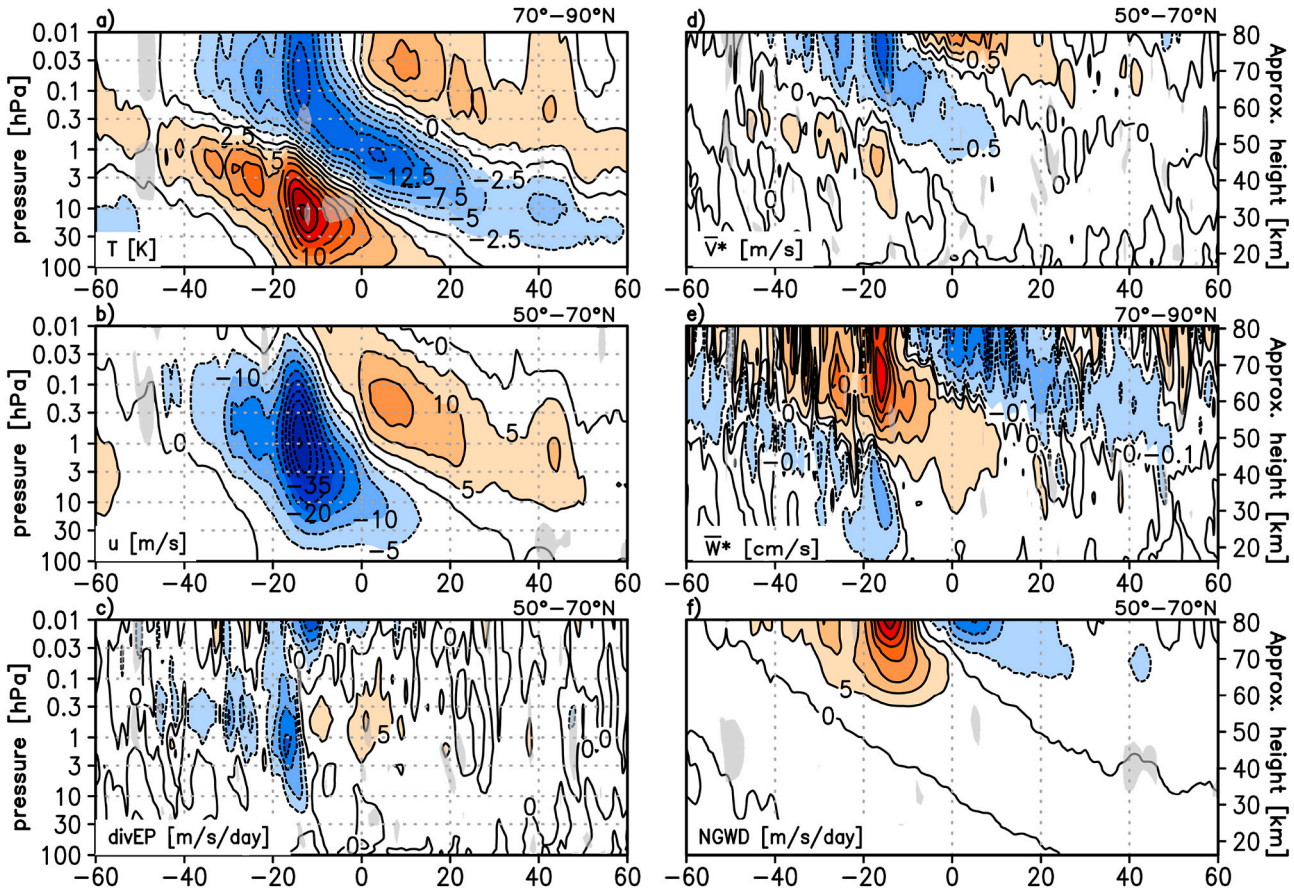

Fig. 4. As Fig. 2 but for the anomalies from the daily climatology of the fields. Gray shading shows where the anomalous SSW-only composite in the REF2000 simulation is significantly different (at a 95% confidence level) from the anomalous SSW-only composite in the REF2095 simulation (compare with Fig. A2) according to a Student's t-test.

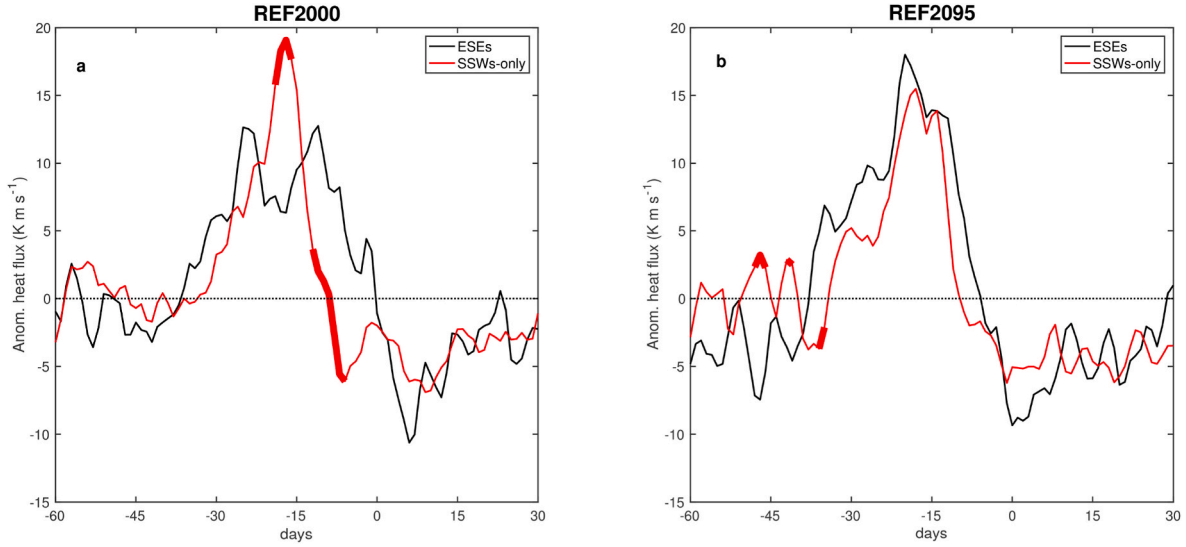

Fig. 5. (a) Composite daily heat flux anomaly [K m/s] averaged between 45° and 75°N at 100 hPa from 60 days before to 30 days after day 0 for ESEs (black line) and SSW-only events (red line) for the REF2000 simulation. (b) Same as (a) but for the REF2095 simulation. The thick lines denote where the ESEs values are significantly different from those of the SSW-only events at a 95% confidence level (Student's t-test).

PW1 in the USLM of the SSW-only composite is likely caused by upward wave propagation, which is possible because the zonal mean zonal wind has already returned to westerlies prior to day 0 (Fig. 2b). Fig. 8b confirms this, as the PW1 seems to be connected to the pre-existing quasi-stationary PW1 and it is only weakened between −14 and −10 day, coincident with easterly winds in lower levels.

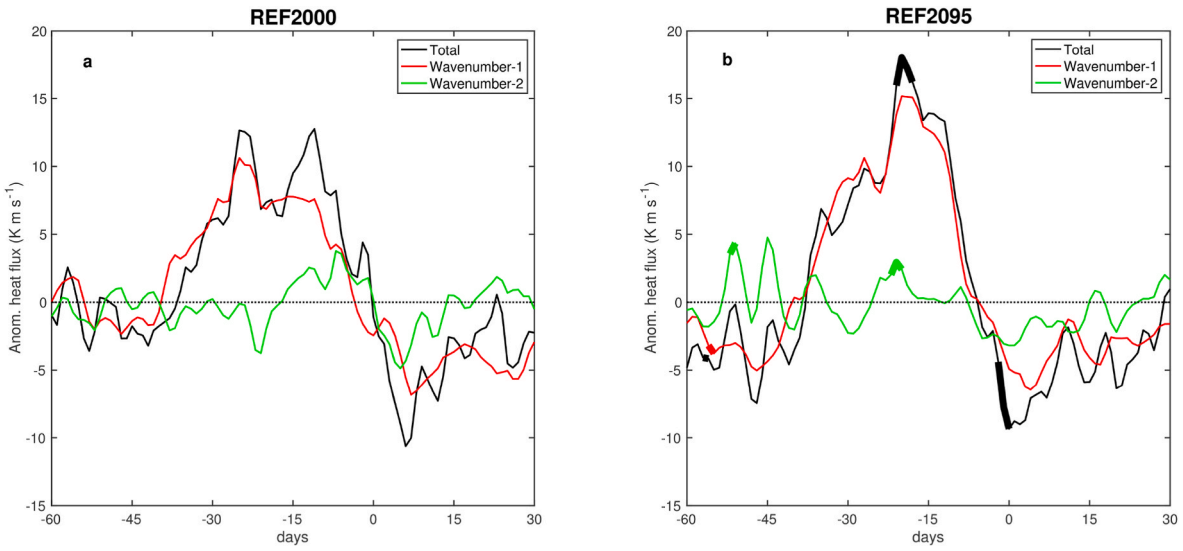

Fig. 6. Composite daily heat flux anomaly [K m/s] averaged between 45° and 75°N at 100 hPa from 60 days before to 30 days after the central date of the ESEs in the (a) REF2000 simulation and (b) REF2095 simulation. Black line: total anomalous flux, red line: wavenumber-1 component, and green line: wavenumber-2 component. Thick lines indicate where the REF2095 values are statistically different from the REF2000 values at a 95% confidence level (Student's t-test).

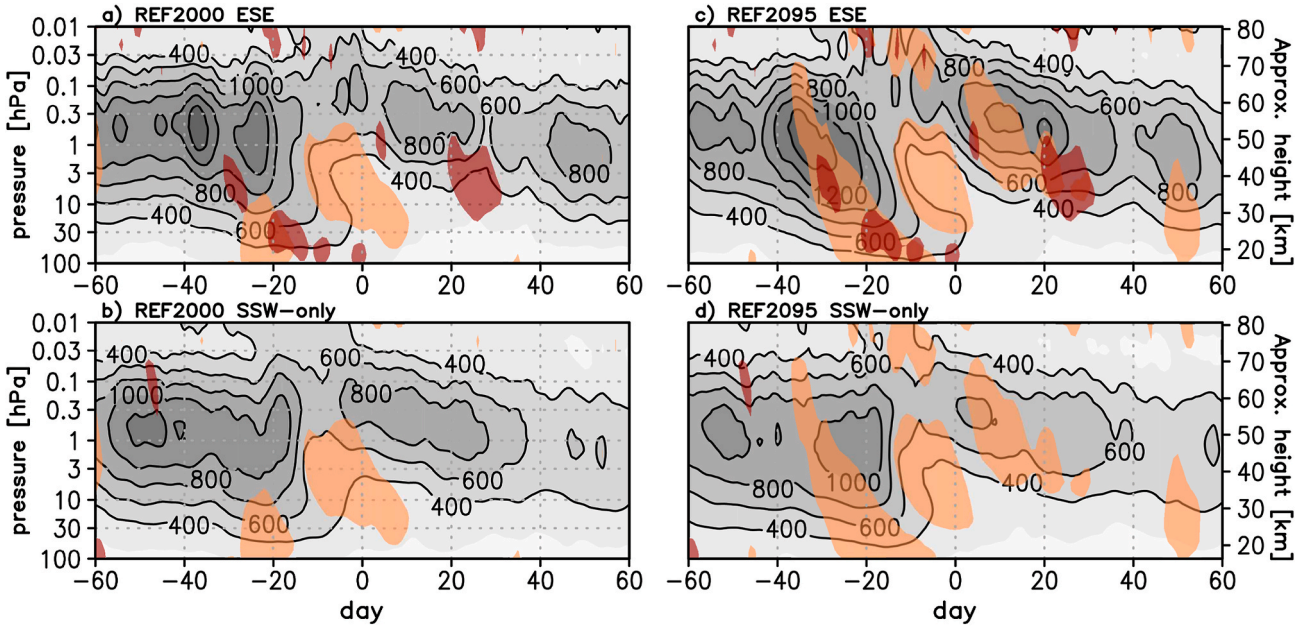

Fig. 7. Composite amplitude of planetary wavenumber-1 of geopotential height (m) at 50°–70°N for a) ESEs and b) SSW-only events in the REF2000 simulation and c) ESEs and d) SSW-only events in the REF2095 simulation. Orange shading denotes where values for ESEs are statistically significantly different from those for SSW-only events at a 95% confidence level (Student's t-test). Red shading denotes where REF2095 composites are different from REF2000 composites at a 95% confidence level (Student's t-test).

4. Future changes in ESEs

In the REF2095 run, SSWs occurred in 33 out of 39 winters (85%), 14 of them (36%) were accompanied by an ESE and the remaining 19 (49%) are considered as SSW-only (Table 1). In this run, events with a change in stratopause height above 9.7 km are declared as ESEs, corresponding to a larger elevation than in REF2000 (8.43 km) (please recall that our ESE definition depends on the climatology of the stratopause jump, as explained in Section 2). This is equivalent to a (non-significant) 12% increase in ESEs from 2000 to 2095. Note that in 24 of the 39 REF2095 winters (62%) the elevation of the stratopause exceeds the ESE criterion of REF2000 (8.43 km), which would imply a 38% increase of winters with ESEs in the future for a static threshold. As for the classification of SSWs, there are no statistically significant changes in the ratio of vortex split SSWs to displacement SSWs for both ESEs and SSW-only events in the future.

Regarding the background state of the middle atmosphere (Figs. 1a, 2a and 9a, A1a) we find lower temperatures in the USLM for the composites of ESEs and SSW-only events in the future than at present. This is related to an enhanced radiative cooling by the future increase in GHG concentrations (e.g., Oberländer et al., 2013; Langematz et al., 2014).

As for ESEs, their specific characteristics, identified under present conditions, remain in general valid in the future (Figs. 1 and 3 and Figs. 9 and 10). However, the anomalies of the respective quantities from the climatological background reveal distinct changes in the future. It is found that the SSW-only events usually develop after

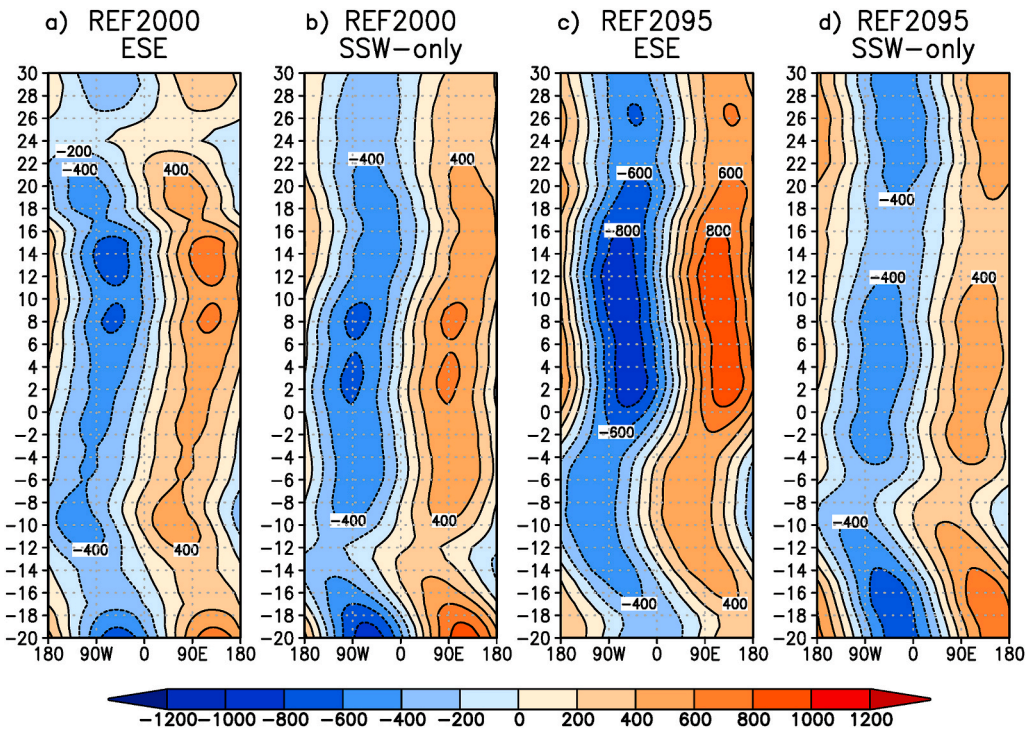

Fig. 8. Hovmöller plots of planetary wavenumber-1 geopotential height (m) at 50°–70°N and 0.2 hPa for a) ESEs and b) SSW-only events in the REF2000 simulation and c) ESEs and d) SSW-only events in the REF2095 simulation. Contour intervals are 200 m. The vertical axis denotes the days relative to the occurrence of the ESE (day 0).

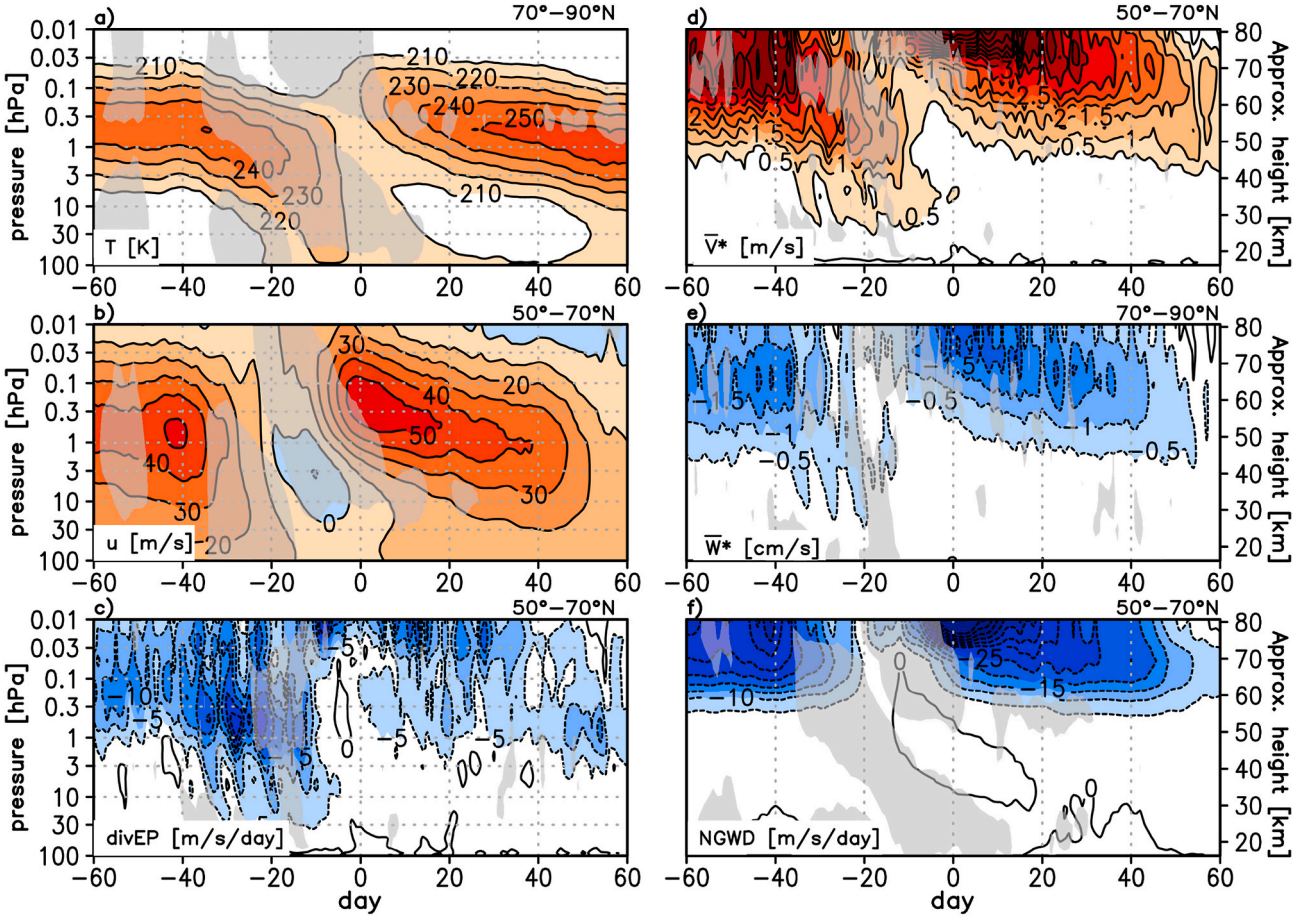

Fig. 9. As in Fig. 1 but for ESEs in the REF2095 simulation.

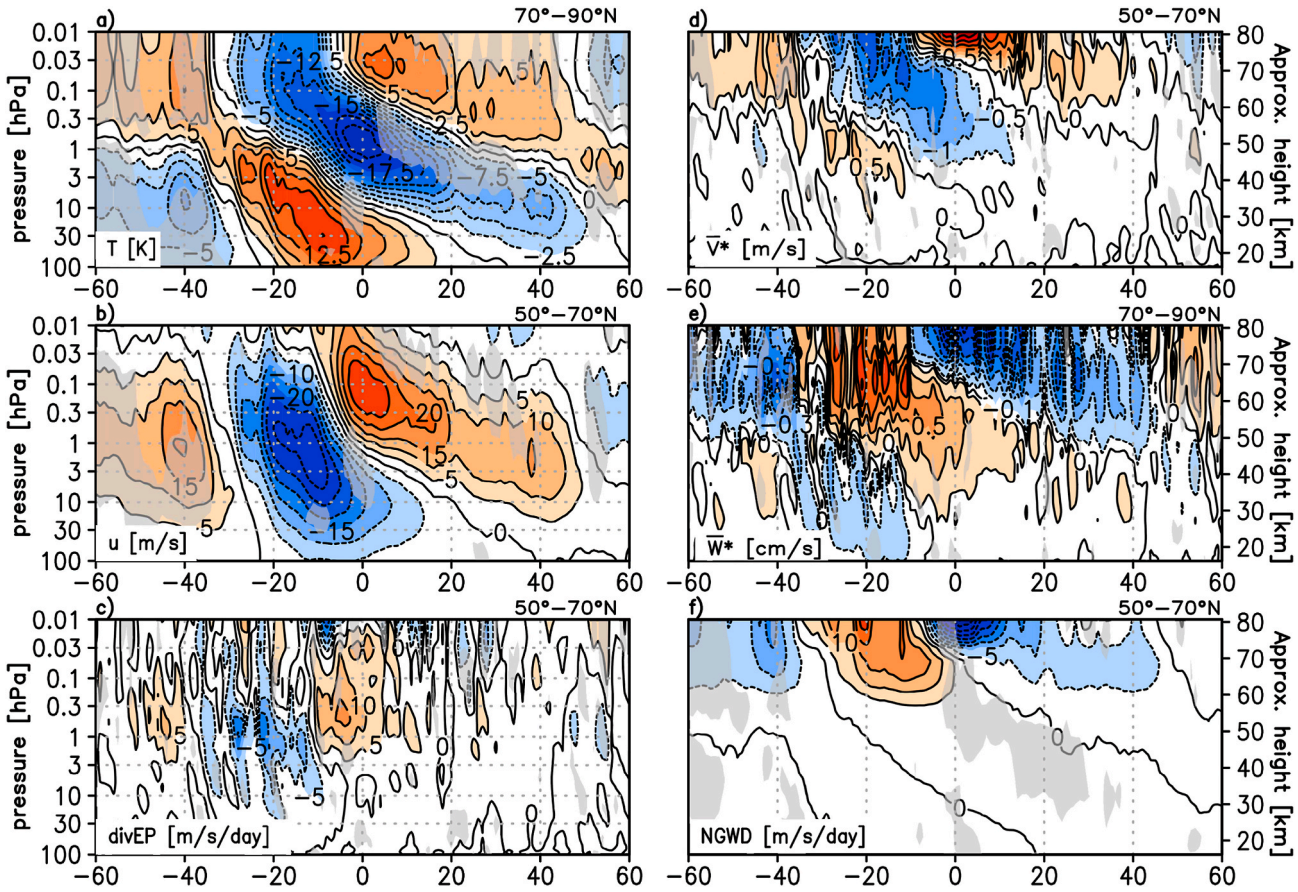

Fig. 10. As in Fig. 3 but for ESEs in the REF2095 simulation.

significantly weak, preconditioned polar vortices in the future simulations (Figs. 9 and 10 and Figs. A1, A2). In contrast, future ESEs are preceded by significantly cold and intense polar vortices in the stratosphere (Figs. 3a, b and 10a, b). This is closely related to future changes in the tropospheric wave forcing. ESEs in the REF2095 simulation develop after a persistently intense eddy heat flux at 100 hPa, as ESEs do in the REF2000 run (Fig. 5b). The peak of the prolonged anomalous HF100, however, is significantly stronger and shorter in the future than in the current climate and stronger than for SSW-only events (not shown). The relative role that the PW2 tropospheric wave forcing played for the build-up of the ESEs in REF2000 by elongating the tropospheric wave driving (days −15 to 0, Fig. 6a) decreases in the future (Fig. 6b), and it is the intense PW1 pulse that is responsible for the appearance of stratospheric easterlies within only 10 days. This result agrees well with other EMAC studies that have shown a future enhancement of PW1 wave activity: Ayarzagüena et al. (2013) projected a future increase in SSW frequency in mid-winter as a result of GHG-induced changes in tropical SSTs. SST changes lead to a strengthening of the tropospheric wave forcing caused by an intensification of the PW1 stationary wave due to a strengthening of the Aleutian low (Ayarzagüena et al., 2013; Oberländer et al., 2013). Later, Ayarzagüena et al. (2015) showed that the changes in the PW1 stationary waves also impact on the anomalous wave forcing preceding SSWs that becomes stronger in the future. The interaction between climatological and anomalous wave components becomes more effective and thus, stronger.

The higher HF100 peak for future ESEs is consistent with high values of EP flux convergence at lower altitudes and explains the faster deceleration of the westerly winds in the stratosphere compared to present ESEs (Figs. 9b, c and 1b, c). This leads to an enhanced downwelling further down in the stratosphere around days −20 and −10 and thus, a deeper descent of the initial stratopause. Therefore, the frequency of future ESEs increases when applying the threshold of the altitude change of the stratopause from the current climate.

Future changes in ESE characteristics are also found during and after their onset. In particular, the positive temperature anomalies in the stratosphere prior to day 0 descend faster in the future than in the past due to an enhancement of the residual downward velocity (Fig. 10e) and they become significantly weaker in the middle and lower stratosphere just before day 0 (Figs. 3a and 10a). These results indicate that the downward propagation of the warm anomaly during the stratopause descent is significantly faster in the future during the ESEs.

The stronger deceleration of the westerly jet prior to ESEs in the future affects the filtering of NGWs. As a result, a significantly weaker and shorter future anomalous eastward NGWD is detected in the USLM from day −3 to day +15, consistent with a weaker upward RC in the USLM (Figs. 3e, f and 10e, f) and resulting in a significantly weaker cooling in that height area around days +3 to +18 (Figs. 3a and 10a) and a shorter duration of the anomalous RC. This future weakening and shortening of the anomalous circulation results in a faster descent of the newly-built stratopause to its climatological height after the ESE. As a counterpart in the upper mesosphere, we find that the newly-built stratopause is colder in the future (Figs. 3a and 10a) as a result of a significantly weaker future anomalous downward circulation at the ESE onset (Figs. 3e and 10e). The lower stratopause temperature in the future may also be influenced by a global weakening of the mesospheric branch of the BDC as shown by Oberländer et al. (2013) for the same EMAC simulations as used in this study. They found a decrease in the residual mean mass stream function above 0.1 hPa and a reduction of the poleward and downward RC in future boreal winter.

Regarding the evolution of the PW1 amplitude in the future, the stratospheric maximum descends significantly more strongly for ESEs than for SSW-only events. This maximum also persists longer in the

middle and lower stratosphere for the ESEs than for the SSW-only events (Fig. 7c and d). In the future, a significantly stronger PW1 amplitude between 40 and 20 days before the ESE (Fig. 7c) is accompanied by a stronger forcing through EP flux convergence than in the past (Fig. 10c). It is also consistent with the predominance of the PW1 component of HF100 for the triggering of SSWs (Fig. 6). Similar to the REF2000 simulation, we also find a pronounced PW1 in the USLM in association with ESEs in the REF2095 simulation, whereas it is much weaker in the SSW-only events (Fig. 7c). The in-situ generation of PWs might again be the origin of the mesospheric PW1 as a travelling PW1 is detected in the LM from −16 days until −10 days (Fig. 8c). In contrast, upward propagation of PW1 is the main cause of the PW1 signal in the mesosphere in the future SSW-only composite as is the case in the present and no travelling waves are detected (Fig. 8d).

5. Summary and discussion

In this study we analyzed the occurrence frequency, characteristic features, and driving mechanisms of ESEs in two multi-year time slice simulations with the EMAC CCM for the years 2000 and 2095.

We have shown that for year 2000 conditions ESEs occur in 24% of the boreal winters. This result is in good agreement with NASA's Modern-Era Retrospective Analysis for Research and Applications (MERRA) reanalysis data of the period 1979–2012 (31%) and results obtained from simulations with the WACCM CCM of the period 1953–2006 (32%) (Chandran et al., 2013a). Most ESEs in EMAC develop after major SSWs, as also reported by Orsolini et al. (2010) and Chandran et al. (2013a).

By relating temperature and zonal wind anomalies to changes in the wave driving and RC, we have shown that EMAC reproduces the main characteristics of ESEs, namely, upward displacements of the stratopause following prolonged zonal wind reversal in the LS, with strong mesospheric cooling, followed by downward propagation of the newly-built stratopause. The sequence of events leading to an ESE can be described as follows:

1. While SSWs (without ESEs) usually follow a longer preconditioning of the mesospheric polar vortex, with positive temperature and easterly wind anomalies progressing downward to the stratosphere, ESEs occur after SSWs preceded by a climatological polar vortex and develop simultaneously in the upper stratosphere and mesosphere. This tendency towards more stable vortices before ESEs than before SSW-only cases agrees with results of Chandran et al. (2013a) for the WACCM CCM.
2. SSWs with ESEs are triggered by a persistent anomalous injection of tropospheric wave activity. In the current climate, this injection was found to be driven by a combination of PW1 and PW2 activity both leading to the characteristic extended wind reversal in the stratosphere.
3. The duration in the tropospheric wave forcing was found to be a key parameter for the development of either an ESE or an SSW-only event. In the ESE case, the tropospheric combined PW1 and PW2 forcing induces a wind reversal in the middle and lower stratosphere that persists 10 days longer than the wind reversal associated with SSW-only events. This leads to differences in the PW drag in the USLM (less in ESEs), in the re-establishment of the polar vortex and the westerly jet (faster and stronger for ESEs), in the resulting westward NGWD (stronger in ESEs), and finally in the re-establishment of the poleward downward circulation in the mesosphere (stronger in ESEs). After ESEs, the maximum sinking over high latitudes is stronger and located higher in the upper mesosphere than before the events; through adiabatic warming of the mesosphere a new higher located stratopause is established.

In addition to the tropospheric wave forcing of ESEs, the onset of the ESE was supported by an enhancement of the PW1 amplitude in the USLM which could be explained with in-situ wave generation. This PW1 dissipates in the upper mesosphere where it exerts a negative westward drag on the zonal flow. In their study with a GW resolving GCM, Tomikawa et al. (2012) also showed these features at similar heights and timing.

The above summary of ESE characteristics under present climate conditions in the EMAC CCM provides evidence that although the top of the EMAC model is located near the mesopause, the model is able to well reproduce key features of ESEs identified in observations or simulated by models with a higher top such as WACCM (Chandran et al., 2013a) or with a higher vertical resolution such as KANTO (Tomikawa et al., 2012). Similar conclusions were drawn by Manney et al. (2008) and Chandran et al. (2013a) for reanalysis models that usually cover the same height domain as EMAC. They showed that although the reanalysis models cannot capture the elevated stratopause at ~85 km during ESEs of the high-top WACCM, they are, nevertheless, able to simulate ESEs with an abrupt rise of the stratopause from approximately 45 km (where it descends before the SSWs) to 65 km. As a result, medium-top models, such as EMAC or reanalysis models, are able to reproduce the physical mechanisms leading to the onset and evolution of ESEs. This includes the tropospheric wave forcing, the dissipation of PWs and GWs in the stratosphere and mesosphere, the associated temperature and circulation changes, as well as the resulting elevation of the stratopause. Medium-top models are, however, not capable to simulate the maximum altitude of elevated stratopauses, nor the circulation changes during ESEs in the lower thermosphere and the associated downward transport of trace species, such as nitrogen oxide (NO_x), from the thermosphere into the mesosphere.

The second focus of this study was the appearance of ESEs in a future climate with further increased GHG concentrations and a recovered stratospheric ozone layer. We obtained the following results:

1. For the end of the 21st century (EMAC REF2095 simulation) we find a significant increase in the number of ESEs, when applying the same threshold value for the detection of ESEs as for the REF2000 simulation. While the total number for SSWs has only slightly increased, nearly half of the SSWs will be followed by an ESE. A slightly lower stratopause height before the ESEs leads to an increase in the range of stratopause height changes in future ESEs, and thus in the number of ESEs. The lower stratopause heights are induced by strong westward PW drag at lower levels prior to SSWs due to stronger injection of tropospheric wave activity.
2. In the future, ESEs occur predominantly after SSWs that develop in meteorological background conditions with a more intense and colder polar vortex. As in the present climate, the initiation of such SSWs (without pre-conditioning) requires a strong tropospheric wave forcing with strong effects up to the mesosphere leading ultimately to ESEs.
3. The tropospheric forcing of SSWs with ESEs in the future has a stronger and more pronounced peak than in the present-day simulation, resulting in a faster establishment of easterly winds in the stratosphere. Most of this forcing is due to a strong pulse of PW1 wave activity. The intensification of the PW1 wave activity before SSWs in the future has been previously described by Ayarzagüena et al. (2015) for the same model and associated with a stronger PW1 climatological wave.
4. In agreement with the nature of the tropospheric wave forcing, there is a predominance of vortex displacement SSWs prior to ESEs. Hence, our results for the present and future climate suggest that there is no clear relationship between split SSWs and ESEs, in contrast to Chandran et al. (2013a) results. We therefore presume that the duration of the tropospheric wave forcing is the relevant parameter that generates the conditions for the development of ESEs, regardless of the wavenumber of the wave activity. In the present climate it is the combination of initial PW1 and successive PW2 activity, while in

the future it is strong PW1 activity, which provide the persistent forcing necessary for the generation of ESEs.
5. The more sudden reversal of westerly winds throughout the stratosphere prior to future ESEs affects the wave propagation of resolved and non-resolved waves leading to a shorter duration of ESEs and a colder newly-built stratopause. The future weakening of the mesospheric RC also contributes to a colder newly-built stratopause, apart from the climate change induced cooling.
6. Other main characteristics of ESEs, e.g., the contributions by PWs and GWs to the ESE driving and the generation of in-situ PW1 during the ESEs, are not likely to change in the future.

Finally, we would like to remark that our algorithm for the identification of ESEs is based on the average polar cap temperature similarly to other studies (e.g. De la Torre et al., 2012; Chandran et al., 2013a). However, France and Harvey (2013) reported that the climatological polar stratopause height might change depending on the location of the vortex core as the mean stratopause inside the vortex core tends to be higher than outside that region. Although the difference in the stratopause height might not be high, it would be interesting in a future study to check if the consideration of the zonal asymmetry of the polar stratopause modulates ESEs characteristics.

Declaration of competing interest

The authors declare that they have no known competing financial interests or personal relationships that could have appeared to influence the work reported in this paper.

Acknowledgements

This work was supported by a research cooperation program between Norway and Germany funded by the Deutscher Akademischer Austauschdienst (DAAD) (Project 54537580) and the Research Council of Norway (Grant 216855). JS was supported by the German Bundesministerium für Bildung und Forschung (BMBF)-MiKlip programme (01LP1137B). BA was funded by the European Project 603557-STRATOCLIM under program FP7-ENV.2013.6.1–2. Dr. S. Oberländer and Dr. S. Meul performed the EMAC simulations and helped with useful discussions. We also thank Prof. K. Shibata for sharing his algorithm to identify split and displacement SSWs. Model data for this paper are available on the SHARP data archive at Freie Universität Berlin upon request. The simulations have been performed on the North-German Supercomputing Alliance (HLRN) computer.

Appendix A. Supplementary data

Supplementary data to this article can be found online at https://doi.org/10.1016/j.jastp.2021.105804.

References

Andrews, D.G., Holton, J.R., Leovy, C.B., 1987. Middle Atmosphere Dynamics. Academic, Orlando, FL.

Ayarzagüena, B., Langematz, U., Meul, S., Oberländer, S., Abalichin, J., Kubin, A., 2013. The role of climate change and ozone recovery for the future timing of major stratospheric warmings. Geophys. Res. Lett. 40, 2460–2465. https://doi.org/10.1002/grl.50477.

Ayarzagüena, B., Orsolini, Y.J., Langematz, U., Abalichin, J., Kubin, A., 2015. The relevance of the location of blocking highs for stratospheric variability in a changing climate. J. Clim. 28, 531–549. https://doi.org/10.1175/JCLI-D-14-00210.1.

Ayarzagüena, B., Polvani, L.M., Langematz, U., Akiyoshi, H., Bekki, S., Butchart, N., Dameris, M., Deushi, M., Hardiman, S.C., Jöckel, P., Klekociuk, A., Marchand, M., Michou, M., Morgenstern, O., O'Connor, F.M., Oman, L.D., Plummer, D.A., Revell, L., Rozanov, E., Saint-Martin, D., Scinocca, J., Stenke, A., Stone, K., Yamashita, Y., Yoshida, K., Zeng, G., 2018. No robust evidence of future changes in major stratospheric sudden warmings: a multi-model assessment from CCMI. Atmos. Chem. Phys. 18, 11277–11287. https://doi.org/10.5194/acp-18-11277-2018.

Ayarzagüena, B., Palmeiro, F.M., Barriopedro, D., Calvo, N., Langematz, U., Shibata, K., 2019. On the representation of major stratospheric warmings in reanalyses. Atmos. Chem. Phys. 19, 9469–9484. https://doi.org/10.5194/acp-19-9469-2019.

Ayarzagüena, B., et al., 2020. Uncertainty in the response of sudden stratospheric warmings and stratosphere-troposphere coupling to quadrupled CO_2 concentrations in CMIP6 models. J. Geophys. Res. Atmos. 125 (6), e2019JD032345 https://doi.org/10.1029/2019JD032345.

Baldwin, M.P., Ayarzagüena, B., Birner, T., Butchart, N., Butler, A.H., Charlton-Perez, A. J., et al., 2021. Sudden stratospheric warmings. Rev. Geophys. 59 https://doi.org/10.1029/2020RG000708 e2020RG000708.

Bönisch, H., Engel, A., Birner, T., Hoor, P., Tarasick, D.W., Ray, E.A., 2011. On the structural changes in the BDC after 2000. Atmos. Chem. Phys. 11, 3937–3948. https://doi.org/10.5194/acp-11-3937-2011.

Braesicke, P., Langematz, U., 2000. On the occurrence and evolution of extremely high temperatures at the polar winter stratopause – a GCM study. Geophys. Res. Lett. 27, 1467–1470.

Chandran, A., Collins, R.L., Garcia, R.R., Marsh, D.R., 2011. A case study of an elevated stratopause generated in the Whole Atmosphere Community Climate Model. Geophys. Res. Lett. 38, L08804. https://doi.org/10.1029/2010GL046566.

Chandran, A., Collins, R.L., Garcia, R.R., Marsh, D.R., Harvey, V.L., Yue, J., de la Torre, L., 2013a. A climatology of elevated stratopause events in the whole atmosphere community climate model. J. Geophys. Res. 118, 1234–1246. https://doi.org/10.1002/jgrd.50123.

Chandran, A., Garcia, R.R., Collins, R.L., Chang, L.C., 2013b. Secondary planetary waves in the middle and upper atmosphere following the stratospheric sudden warming event of January 2012. Geophys. Res. Lett. 40 https://doi.org/10.1002/grl.50373.

Charlton, A.J., Polvani, L.M., 2007. A new look at stratospheric sudden warmings. Part I: climatology and modeling benchmarks. J. Clim. 20, 449–469.

Charlton-Perez, A.J., Polvani, L.M., Austin, J., Li, F., 2008. The frequency and dynamics of stratospheric sudden warmings in the 21st century. J. Geophys. Res. 113, D16116. https://doi.org/10.1029/2007JD009571.

De la Torre, L., Garcia, R.R., Barriopedro, D., Chandran, A., 2012. Climatology and characteristics of stratospheric sudden warmings in the whole atmosphere community climate model. J. Geophys. Res. 117, D04110. https://doi.org/10.1029/2011JD016840.

France, J.A., Harvey, V.L., 2013. A climatology of the stratopause in WACCM and the zonally asymmetric elevated stratopause. J. Geophys. Res. 118, 2241–2254. https://doi.org/10.1002/jgrd.50218.

France, J.A., Harvey, V.L., Alexander, M.J., Randall, C.E., Gille, J.C., 2012. High Resolution Dynamics Limb Sounder observations of the gravity wave-driven elevated stratopause in 2006. J. Geophys. Res. 117, D20108. https://doi.org/10.1029/2012JD017958.

Hines, C.O., 1997a. Doppler-spread parameterization of gravity-wave momentum deposition in the middle atmosphere. Part 1: basic formulation. J. Atmos. Sol. Terr. Phys. 59, 371–386. https://doi.org/10.1016/S1364-6826(96)00079-X.

Hines, C.O., 1997b. Doppler-spread parameterization of gravity-wave momentum deposition in the middle atmosphere. Part 2: broad and quasi monochromatic spectra, and implementation. J. Atmos. Sol. Terr. Phys. 59, 387–400. https://doi.org/10.1016/S1364-6826(96)00080-6.

Hitchman, M.H., Gille, J.C., Rodgers, C.D., Brasseur, G., 1989. The separated polar winter stratopause - a gravity wave driven climatological feature. J. Atmos. Sci. 46, 410–422, 10.1175/1520-0469(1989)046 0410:TSPWSA 2.0.CO;2.

Hoskins, B.J., McIntyre, M.E., Robertson, A.W., 1985. On the use and significance of isentropic potential vorticity maps. Quart. J. Roy. Meteor. Soc. 111, 877–946.

Hu, Y., Tung, K.K., 2003. Possible ozone-induced long-term changes in planetary wave activity in late winter. J. Clim. 16, 3027–3038. https://doi.org/10.1175/1520-0442(2003)016<3027:POLCIP>2.0.CO;2.

IPCC, 2001. Climate Change 2001: The Scientific Basis. Contribution of Working Group I to the Third Assessment Report of the Intergovernmental Panel on Climate Change. In: Houghton, J.T., Ding, Y., Griggs, D.J., Noguer, M., van der Linden, P.J., Dai, X., Maskell, K., Johnson, C.A. (Eds.). Cambridge University Press, Cambridge, United Kingdom and New York, NY, USA, p. 881.

Jöckel, P., Tost, H., Pozzer, A., Brühl, C., Buchholz, J., Ganzeveld, L., Hoor, P., Kerkweg, A., Lawrence, M.G., Sander, R., Steil, B., Stiller, G., Tanarhte, M., Taraborrelli, D., van Aardenne, J., Lelieveld, J., 2006. The atmospheric chemistry general circulation model ECHAM5/MESSy1: consistent simulation of ozone from the surface to the mesosphere. Atmos. Chem. Phys. 6, 5067–5104. https://doi.org/10.5194/acp-6-5067-2006.

Jungclaus, J.H., Keenlyside, N., Botzet, M., Haak, H., Luo, J.-J., Latif, M., Marotzke, J., Mikolajewicz, U., Roeckner, E., 2006. Ocean circulation and tropical variability in the coupled model ECHAM5/MPI-OM. J. Clim. 19, 3952–3972. https://doi.org/10.1175/JCLI3827.1.

Karpechko, A.Y., Manzini, E., 2012. Stratospheric influence on tropospheric climate change in the Northern Hemisphere. J. Geophys. Res. 117, D05133. https://doi.org/10.1029/2011JD017036.

Kvissel, O.-K., Orsolini, Y.J., Stordal, F., Limpasuvan, V., Richter, J., Marsh, D.R., 2012. Mesospheric intrusion and anomalous chemistry during and after a major stratospheric sudden warming. J. Atmos. Sol. Terr. Phys. 78–79, 116–124. https://doi.org/10.1016/j.jastp.2011.08.015.

Labitzke, K., 1972. Temperature changes in the mesosphere and stratosphere connected with circulation changes in winter. J. Atmos. Sci. 29, 756–766, 10.1175/1520-0469(1972)029 0756:TCITMA 2.0.CO;2.

Labitzke, K., 1981. The amplification of height wave 1 in January 1979: a characteristic precondition for the major warming in February. Mon. Weather Rev. 109, 983, 10.1175/1520-0493(1981)109h0983:TAOHWIi2.0.CO;2.

Langematz, U., Meul, S., Grunow, K., Romanowsky, E., Oberländer, S., Abalichin, J., Kubin, A., 2014. Future Arctic temperature and ozone: the role of stratospheric composition changes. J. Geophys. Res. Atmos. 119, 2092–2112. https://doi.org/10.1002/2013JD021100.

Limpasuvan, V., Richter, J.H., Orsolini, Y.J., Stordal, F., Kvissel, O.-K., 2012. The roles of planetary and gravity waves during a major stratospheric sudden warming as characterized in WACCM. J. Atmos. Sol. Terr. Phys. 84–98. https://doi.org/10.1016/j.jastp.2011.03.004.

Limpasuvan, V., Orsolini, Y.J., Chandran, A., Garcia, R.R., Smith, A.K., 2016. On the composite response of the MLT to major sudden stratospheric warming events with elevated stratopause. J. Geophys. Res. Atmos. 121 https://doi.org/10.1002/2015JD024401.

Liu, H.-L., Roble, R.G., 2002. A study of a self-generated stratospheric sudden warming and its mesospheric – lower thermospheric impacts using the coupled TIME-GCM/CCM3. J. Geophys. Res. 107, 4695. https://doi.org/10.1029/2001JD001533.

Lott, F., Miller, M.J., 1997. A new subgrid-scale orographic drag parametrization: its formulation and testing. Q. J. R. Meteorol. Soc. 123, 101–127. https://doi.org/10.1002/qj.49712353704.

Manney, G., Krüger, K., Pawson, S., Minschwaner, K., Schwartz, M.J., Daffer, W.H., Livesey, N.J., Mlynczak, M.G., Remsberg, E.E., Russell III, J.M.R., Waters, J.W., 2008. The evolution of the stratopause during the 2006 major warming: satellite data and assimilated meteorological analyses. J. Geophys. Res. 113 (D11115) https://doi.org/10.1029/2007JD009097.

Manney, G.L., Harwood, R.S., MacKenzie, I.A., Minschwaner, K., Allen, D.R., Santee, M. L., Walker, K.A., Hegglin, M.I., Lambert, A., Pumphrey, H.C., Bernath, P.F., Boone, C. D., Schwartz, M.J., Livesey, N.J., Daffer, W.H., Fuller, R.A., 2009a. Satellite observations and modeling of transport in the upper troposphere through the lower mesosphere during the 2006 major stratospheric sudden warming. Atmos. Chem. Phys. 9, 4775–4795. https://doi.org/10.5194/acp-9-4775-2009.

Manney, G.L., Schwartz, M.J., Krüger, K., Santee, M.L., Pawson, S., Lee, J.N., Daffer, W. H., Fuller, R.A., Livesey, N.J., 2009b. Aura Microwave Limb Sounder observations of dynamics and transport during the record-breaking 2009 Arctic stratospheric major warming. Geophys. Res. Lett. 36 (L12815) https://doi.org/10.1029/2009GL038586.

McLandress, C., Shepherd, T., 2009. Impact of climate change on stratospheric sudden warmings as simulated by the Canadian middle atmosphere model. J. Clim. 22, 5449–5463.

McLandress, C., Scinocca, J.F., Shepherd, T.G., Reader, M.C., Manney, G.L., 2013. Dynamical control of the mesosphere by orographic and nonorographic gravity wave drag during the extended northern winters of 2006 and 2009. J. Atmos. Sci. 70, 2152–2169. https://doi.org/10.1175/JAS-D-12-0297.1.

Meul, S., Langematz, U., Oberländer, S., Garny, H., Jöckel, P., 2014. Chemical contribution to future tropical ozone change in the lower stratosphere. Atmos. Chem. Phys. 14, 2959–2971. https://doi.org/10.5194/acp-14-2959-2014.

Mitchell, D., Osprey, S., Gray, L., Butchart, N., Hardiman, S., Charlton-Perez, A., Watson, P., 2012. The effect of climate change on the variability of the northern hemisphere stratospheric polar vortex. J. Atmos. Sci. 69, 2608–2618.

Newman, P.A., Rosenfield, J.E., 1997. Stratospheric thermal damping times. Geophys. Res. Lett. 24, 433–436. https://doi.org/10.1029/96GL03720.

Nissen, K.M., Matthes, K., Langematz, U., Mayer, B., 2007. Towards a better representation of the solar cycle in general circulation models. Atmos. Chem. Phys. 7, 5391–5400.

Oberländer, S., Langematz, U., Meul, S., 2013. Unraveling impact factors for future changes in the Brewer-Dobson circulation. J. Geophys. Res. 118 (10) https://doi.org/10.1002/jgrd.50775, 296–10,312.

Orsolini, Y.J., Urban, J., Murtagh, D.P., Lossow, S., Limpasuvan, V., 2010. Descent from the polar mesosphere and anomalously high stratopause observed in 8 years of water vapor and temperature satellite observations by Odin Sub-Millimeter Radiometer. J. Geophys. Res. 115 (D12305) https://doi.org/10.1029/2009JD013501.

Orsolini, Y.J., Limpasuvan, V., Perot, K., Espy, P.J., Hibbins, R.E., Lossow, S., Larsson, K. R., Murtagh, D., 2017. Modelling the descent of nitric oxide during the elevated stratopause event of January 2013. J. Atmos. Sol. Terr. Phys. 155, 50–61.

Plumb, R.A., 2002. Stratospheric transport. J. Meteorol. Soc. Jpn. 80, 793–809. https://doi.org/10.2151/jmsj.80.793.

Ren, S., Polavarapu, S., Beagley, S.R., Nezlin, Y., Rochon, Y.J., 2011. The impact of gravity wave drag on mesospheric analyses of the 2006 stratospheric major warming. J. Geophys. Res. 116, D19116. https://doi.org/10.1029/2011JD015943.

Roeckner, E., Brokopf, R., Giorgetta, M., Hagemann, S., Kornblueh, L., 2006. Sensitivity of simulated climate to horizontal and vertical resolution in the ECHAM5 atmosphere model. J. Clim. 19, 3771–3791. https://doi.org/10.1175/JCLI3824.1.

Sander, R., Kerkweg, A., Jöckel, P., Lelieveld, J., 2005. Technical note: the new comprehensive atmospheric chemistry module MECCA. Atmos. Chem. Phys. 5, 445–450.

Siskind, D.E., Eckermann, S.D., Coy, L., McCormack, J.P., Randall, C.E., 2007. On recent interannual variability of the Arctic winter mesosphere: implications for tracer descent. Geophys. Res. Lett. 34, L09806. https://doi.org/10.1029/2007GL029293.

Smith, A.K., 2003. The origin of stationary planetary waves in the upper mesosphere. J. Atmos. Sci. 60, 3033–3041. https://doi.org/10.1175/1520-0469(2003)060<3033:TOOSPW>2.0.CO;2.

Smith, A.K., Lopez-Puertas, M., Garcia-Comas, M., Tukiainen, S., 2009. SABER observations of mesospheric ozone during NH late winter 2002-2009. Geophys. Res. Lett. 36 (L23804) https://doi.org/10.1029/2009GL040942.

Stray, N.H., Orsolini, Y.J., Espy, P.J., Limpasuvan, V., Hibbins, R.E., 2015. Observations of planetary waves in the mesosphere-lower thermosphere during stratospheric warming events. Atmos. Chem. Phys. 15 (9), 4997–5005. https://doi.org/10.5194/acp-15-4997-2015.

Tomikawa, Y., 2010. Persistence of easterly wind during major stratospheric sudden warmings. J. Clim. 23, 5258–5267. https://doi.org/10.1175/2010JCLI3507.1.

Tomikawa, Y., Sato, K., Watanabe, S., Kawatani, Y., Miyazaki, K., Takahashi, M., 2012. Growth of planetary waves and the formation of an elevated stratopause after a major stratospheric sudden warming in a T213L256 GCM. J. Geophys. Res. 117, D16101. https://doi.org/10.1029/2011JD017243.

Tweedy, O., Limpasuvan, V., Orsolini, Y.J., Smith, A.K., Garcia, R.R., Kinnison, D., Randall, C.E., Kvissel, O.-K., Stordal, F., Harvey, V.L., Chandran, A., 2013. Nighttime secondary ozone layer during major stratospheric sudden warmings in specified-dynamics WACCM. J. Geophys. Res. Atmos. 118 https://doi.org/10.1002/jgrd.50651.

World Meteorological Organization, 1957. Meteorology — a three-dimensional science: second session of the commission for aerology. World Meteorol. Organ. Bull. IV (4), 134–138.

World Meteorological Organization (WMO), 2007. Scientific Assessment of Ozone Depletion: 2006, vol. 50. Global Ozone Research and Monitoring Project-Report, Geneva, Switzerland.

Zhang, J., Limpasuvan, V., Orsolini, Y.J., Espy, P.J., Hibbins, R.E., 2021. Climatological westward propagating semidiurnal tides and their composite response to sudden stratospheric warmings in SuperDARN and SD-WACCM-X. J. Geophys. Res. Atmos. 126 https://doi.org/10.1029/2020JD032895 e2020JD032895.